All-optical injection and detection of ballistic charge currents in germanium

Eric J. Loren,[1] Hui Zhao,[2] and Arthur L. Smirl[1,a)]
[1]*Laboratory for Photonics and Quantum Electronics, 138 IATL, University of Iowa, Iowa City, Iowa 52242, USA*
[2]*Department of Physics and Astronomy, The University of Kansas, 2063 Malott Hall, 1251 Wescoe Hall Dr., Lawrence, Kansas 66045, USA*

(Received 17 July 2010; accepted 13 September 2010; published online 26 October 2010)

All optical techniques are used to inject and to study the relaxation dynamics of ballistic charge currents in clean germanium at room temperature without the application of external contacts or the use of externally applied fields. Ballistic currents are injected by the quantum interference between the transition amplitudes for direct one and two photon absorption of a pair of phase-locked and harmonically related ultrafast laser pulses. The transport of carriers following ballistic injection is temporally and spatially resolved using optical differential transmission techniques that are sensitive to the relative optical phase of the two injection pulses. The electron-hole dynamics are determined by the initial ballistic injection velocity, momentum relaxation, and space charge field effects. The injection process in Ge is similar to that in direct band gap materials but the indirect nature of Ge complicates the monitoring of the carrier dynamics, allowing the holes to play a more prominent role than in direct gap materials. The latter opens the possibility of following the hole (as opposed to the electron) dynamics. © *2010 American Institute of Physics*. [doi:10.1063/1.3500547]

I. INTRODUCTION

Thermalized transport (i.e., drift and diffusion) driven by an electric field, magnetic field or by a density gradient has formed the foundation of semiconductor device physics. However, device dimensions have reached the 20 nm level, where transport over dimensions comparable to the mean free path of the electrons and on time scales comparable to the momentum relaxation time can no longer be ignored. Future progress depends, in part, on our ability to control such ballistic currents, and that control, in turn, depends upon developing techniques that allow us to generate and detect ballistic currents and to study and understand charge movement with femtosecond temporal and nm spatial resolution in technologically relevant materials.

We have recently demonstrated the feasibility of a platform for injecting ballistic charge currents into semiconductors and measuring their relaxation dynamics.[1] The ballistic charge currents are injected by the interference between two photon absorption of a linearly-polarized fundamental pulse with frequency ω and the single-photon absorption of the corresponding second harmonic pulse at 2ω with the same polarization.[1–8] These quantum interference and control (QUIC) techniques are noninvasive—not requiring the use of electrodes or externally applied fields—and they allow precise control of the injected currents. The polarization direction of the harmonically-related pulses dictates the direction of that current flow, while the relative phase between the two pulses determines the magnitude of the current. The electrons (holes) comprising these currents are injected into the conduction (valence) band with a large initial velocity, which requires no external accelerating force and which can be controlled by choosing the excitation energy, $2\hbar\omega$.

Once injected, the carriers move ballistically with this velocity until the momentum relaxes on subpicosecond time scales. For typical injection velocities and momentum relaxation times, this corresponds to a mean free path for the electrons and holes of ~100 nm or less. By comparison, the tightly-focused, diffraction-limited optical pulses used here have a diameter of a few microns—at least an order of magnitude larger than the mean free path. Nevertheless, (as described previously[1] and below), these pulses can be used to follow the carrier motion over nm dimensions and on femtosecond time scales by measuring the phase-dependent differential transmission. The advantage of this technique is that the height of the phase-dependent derivative indicates the distance that the carriers move, thereby, removing the need for high spatial resolution from the focused probe pulse.

GaAs was chosen for these initial studies because it is a direct band gap material and because it is the semiconductor most frequently used for photonic applications, and therefore, is relatively well-characterized. On the other hand, the most common materials for electronic (i.e., transport) applications are the group IV semiconductors, especially Si. However, group IV materials are seldom used for photonic applications, primarily because they are indirect band gap semiconductors, and consequently, interact weakly with light and because they exhibit inversion symmetry, and therefore, have a vanishing second order nonlinear optical susceptibility. Because of the lattice mismatch between GaAs and Si, GaAs is not an attractive candidate for monolithic electronic-photonic integration. By comparison, Ge is a pseudodirect gap semiconductor (i.e., it has a small difference between Γ and L bandgaps) that has been successfully grown on Si. Even though Ge is an indirect gap semiconductor, the direct transitions at Γ (near the center of the Brillouin zone) can be readily accessed and have been shown to produce strong electro-optical and nonlinear optical responses, such as the

a)Electronic mail: art-smirl@uiowa.edu.

quantum confined Stark effect[9] and transient gain,[10,11] respectively. For this reason, the photonics community has recently shown a renewed interest in Si–Ge structures, and here, we show that our platform[1] can be used to inject and detect ballastic currents in Ge.

Recently, charge currents in Ge produced by quantum interference have been detected by observing the terahertz (THz) radiation emitted by such currents.[12] THz experiments detect radiation that is generated by charge acceleration; therefore, they are extremely sensitive to transient currents. By comparison, the measurements reported here track the change in the position of the charge as a function of time. In this way, they provide complementary information. As an example of how this information can be useful, consider that the experimental data in Ref. 12 are consistent with either optical rectification (associated with the real part of $\chi^{(3)}$) or the injection of an electrical current (associated with the imaginary part of $\chi^{(3)}$). While arguments can be made as to why one might expect an injection current rather than optical rectification, the measurements presented in this paper show conclusively that charge is injected and that it moves macroscopic distances—inconsistent with optical rectification.

The paper is organized as follows. In Sec. II, the process and apparatus for injecting ballistic currents in Ge by quantum interference are described, and we identify parameters that can be used to characterize the carrier motion: the height and width of the electron and hole spatial profiles and the phase and time dependent peak changes in electron and hole densities. In Sec. III, we demonstrate the measurement of the height and the width of the injected carrier distributions using conventional phase-independent differential transmission techniques and verify that we are operating in the linear regime with respect to carrier density. Next, in Sec. IV, we describe the measurement of the phase-dependent differential transmission, which allows the extraction of the peak changes in the electron and hole densities caused by the ballistic current injection. The results of Secs. III and IV together then allow the extraction of values for the average distance moved per carrier (considering both electrons and holes). Results and conclusions are summarized in Sec. V.

II. INJECTION OF BALLISTIC CURRENTS

For the generation of ballistic charge (electrical) currents in Ge, we take advantage of the interference between two photon absorption of ~250 fs pulses at 1760 nm and single photon absorption of the second harmonic at 880 nm. As shown in Fig. 1(a), the fundamental (ω) pulse is the idler of an optical parametric oscillator (OPO) pumped by a Ti:sapphire laser at 80 MHz, and the second harmonic (2ω) is generated by frequency doubling in a beta barium borate crystal. A scanning dichroic interferometer controls the difference, $\phi_\omega - \phi_{2\omega}$, between the phases of the ω and 2ω pulses. Subsequently, the pulses are collinearly recombined and tightly-focused onto the sample surface. The polarizations of the pulses are arranged to be collinear (along $\hat{x}$) by polarizers and waveplates not shown in Fig. 1(a).

The currents are injected into an undoped 1-μm-thick layer of bulk germanium at room temperature. The sample

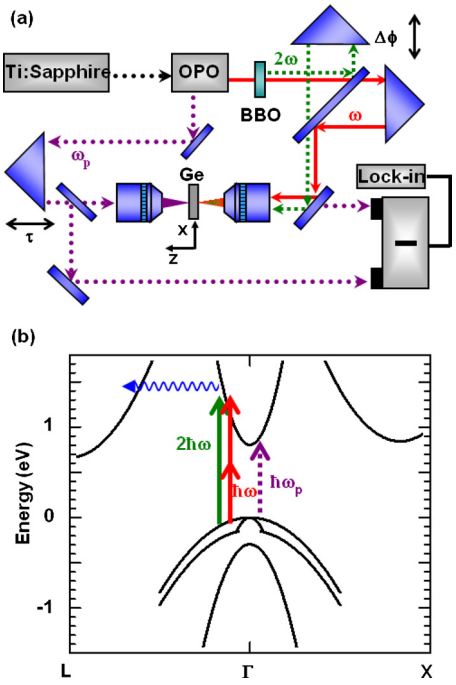

FIG. 1. (Color online) (a) Experimental apparatus for injecting and detecting charge currents. (b) Schematic of the key features of the Ge bandstructure, with the two photon absorption of the ω pulse and one photon absorption of the 2ω pulse indicated by the solid arrows and with the direct absorption of the probe (ω_p) shown as a dashed arrow. Phonon-assisted scattering to the side valleys is indicated by a wavy arrow.

was prepared from a 2-mm-thick slice of Czochralski-grown single crystal Ge (minimum resistivity 40 Ω cm) with the $\langle 111 \rangle$ plane as the face. The crystal was mechanically polished on one side, etched and bonded to a fused silica substrate (BK7 glass) using a glue that is transparent to wavelengths used here. The second surface was then polished until the wafer was ~10 μm thick and subsequently etched to a thickness of ~6 μm. Finally, the sample was ion-milled to a thickness of ~1 μm, as determined by optical interferometric techniques.

The relevant features of the Ge bandstructure at room temperature are sketched in Fig. 1(b). The direct band gap (E_Γ=0.805 eV) is at the Γ point; the four lowest indirect valleys at L (E_L=0.664 eV); and six higher valleys at X (E_X=0.844 eV). One photon absorption of the 2ω pulse ($2\hbar\omega$=1.41 eV) directly couples states in the direct Γ-conduction band valley to states in the heavy-hole (hh), light-hole (lh), and split off (so) valence bands. For example, the hh valence-to-conduction band transitions inject electrons (holes) into the Γ-valley (hh band) with an excess energy of ~542 meV (~64 meV), corresponding to a ballistic injection speed of ~2000 km/s (~200 km/s). These excess energies and speeds are much larger than in our earlier experiments[1,6,7] in GaAs. Once created, the electrons scatter via long wave vector phonons from the central Γ-conduction band valley to the four lower L-conduction side valleys in ~200 fs,[13–15] a time comparable to, but shorter than, our temporal resolution. For the fluences discussed here (0.1–5 μJ/cm^2), one photon absorption ($\alpha^{2\omega} \sim 3 \times 10^4$ cm^{-1}) (Ref. 16) creates peak electron-hole pair densities in the range of 10^{16}–5×10^{17} cm^{-3}. The carrier spatial

profiles generated by absorption of the 2ω pulse are ~ Gaussian shaped in the plane of the sample with a diameter of ~3 μm (full width at half maximum, FWHM), and the carrier densities decrease exponentially in the propagation ($\hat{z}$) direction with a characteristic length of ~333 nm. Indirect transitions are also energetically allowed but are weak compared to the direct transitions.

By comparison, two photon absorption of the ω-pulse ($\hbar\omega$=0.706 eV) couples the same states in the valence and conduction bands as one photon absorption of the 2ω-pulse. In addition, phonon-assisted indirect absorption of the ω-pulse is allowed, and it competes with (and is detrimental to) the quantum interference process described below. Using values from the literature for the indirect (α^{ω}_{ID}=25 cm^{-1}) (Ref. 16) and the two photon (β^{ω}=100 cm/GW, as scaled from Ref. 14 using Ref. 17) absorption coefficients, one can estimate the fluence (~180 μJ/cm^2) at which these two processes produce equal carrier densities (~2×10^{16} cm^{-3}). Once carriers are created, free carrier absorption (FCA) also occurs, whereby an electron absorbs a photon and emits or absorbs a phonon. We can estimate the strength of FCA by writing the absorption coefficient as $\alpha^{\omega}_{\mathrm{FCA}}=(\sigma^{e}_{\mathrm{FCA}}+\sigma^{h}_{\mathrm{FCA}})N$, where $\sigma^{e}_{\mathrm{FCA}}\sim5\times10^{-18}$ cm^2 and $\sigma^{h}_{\mathrm{FCA}}\sim7\times10^{-18}$ cm^2 are the FCA absorption cross sections for the electrons and holes, respectively (scaled from Ref. 18), and N is the carrier density. For peak carrier densities of ~10^{17} cm^{-3}, $\alpha^{\omega}_{\mathrm{FCA}}$ ~1 cm^{-1}, and FCA is always less important than either indirect or two-photon absorption.

When both ω and 2ω pulses are simultaneously present, the interference between one and two photon absorption is known to inject a charge (or electrical) current into the semiconductor of the form:[3,19,20] $dJ_i/dt=2\eta_{ijkl}E^{\omega}_j E^{\omega}_k E^{2\omega}_l \sin(\Delta\phi)$ (where E^{ω} and $E^{2\omega}$ are the slowly varying field envelopes of the two pump pulses; $\Delta\phi=2\phi_{\omega}-\phi_{2\omega}$; η_{ijkl} is a fourth-order tensor that is related to the imaginary part of the third-order nonlinear susceptibility; and the subscripts i, j, k, and l denote the crystallographic axes).

The net effect of the simultaneous one and two photon absorption of the 2ω and ω pulses (and the accompanying quantum interference) is to produce a *local* density profile $N_{e(h)}(\Delta\phi,x,y,t)$ for the electrons (e) and holes (h) whose position and shape at a later time t depend upon the relative phases $\Delta\phi$ of the two pump pulses at the time of injection. The electrons and holes are initially injected with identical spatial profiles $N_e(\Delta\phi,x,y,t=0)=N_h(\Delta\phi,x,y,t=0)$ with width $W(t=0)$ (FWHM) and with peak amplitude $N_e(\Delta\phi,x=0,\ y=0,\ t=0)=N_h(\Delta\phi,x=0,\ y=0,\ t=0)$, independent of $\Delta\phi$, as indicated by the dashed Gaussian-shaped line in Fig. 2(a). For ω and 2ω co-polarized along $\hat{x}$, the holes and electrons are ballistically injected with oppositely directed average velocities, $\langle v_e(t=0)\rangle\sin\Delta\phi$ and $\langle v_h(t=0)\rangle\sin\Delta\phi$, respectively, as indicated by the arrows in Fig. 2(a).[3,6,19] We emphasize that $\langle v_{e(h)}(t=0)\rangle$ is the *average* velocity per electron (hole), and the averaging takes into account that not all of the injected carriers are generated by the quantum interference process, and of the fraction that are part of the current, not all are injected with velocities directed along $\hat{x}$.

If the average distance moved per electron (hole) $x_{e(h)}$ is small compared to the width of the profile (i.e., $x_{e(h)}\ll W$) then the electron and hole profiles can be written as

$$N_{e(h)}(\Delta\phi;x,y;t)=N_{e(h)}(\Delta\phi=0;x,y;t)-x_{e(h)}(\Delta\phi;t)\times[\partial N_{e(h)}(\Delta\phi=0;x,y;t)/\partial x], \quad (1)$$

where $e(h)$ as usual refers to the electrons (holes). Thus, the difference between the profiles with and without current injection $\Delta N_{e(h)}(\Delta\phi;x,y;t)\equiv N_{e(h)}(\Delta\phi;x,y;t)-N_{e(h)}(\Delta\phi=0;x,y;t)$, is proportional to the derivative of the original profile, and the height of the derivative is proportional to the average distance each electron (hole) has moved, as depicted in Fig. 2. Under these circumstances, it is straight forward to show that for a Gaussian pump beam profile

$$x_{e(h)}(\Delta\phi;t)=\frac{1}{2}\sqrt{\frac{e}{2\ln 2}}\frac{\Delta N_{e(h)}(\Delta\phi;x=x_{\mathrm{inf}},\ y=0;t)}{N_{e(h)}(\Delta\phi=0;\ x=0,\ y=0;t)}W(t)=\frac{1}{2}\sqrt{\frac{e}{2\ln 2}}\frac{\Delta N^{0}_{e(h)}(\Delta\phi;t)}{N_0(t)}W(t), \quad (2)$$

where e=2.718 and where $W(t)$ and $N_0(t)\equiv N_{e(h)}(\Delta\phi=0;0,0;t)$ are the width (FWHM) and height, respectively, of the electron and hole density profiles in the absence of current injection, although (as we will show in Sec. III) current injection ($\Delta\phi\neq0$) does not change these two parameters measurably. $\Delta N^{0}_{e(h)}(\Delta\phi;t)\equiv\Delta N_{e(h)}(\Delta\phi;x_{\mathrm{inf}},0;t)$ denotes the peak of the derivative, which occurs at the inflection point of the Gaussian profile, $x_{\mathrm{inf}}=W/[2\sqrt{2\ln 2}]$. Notice that the initial sign of $x_{e(h)}$ is determined by the injection velocity [i.e.,

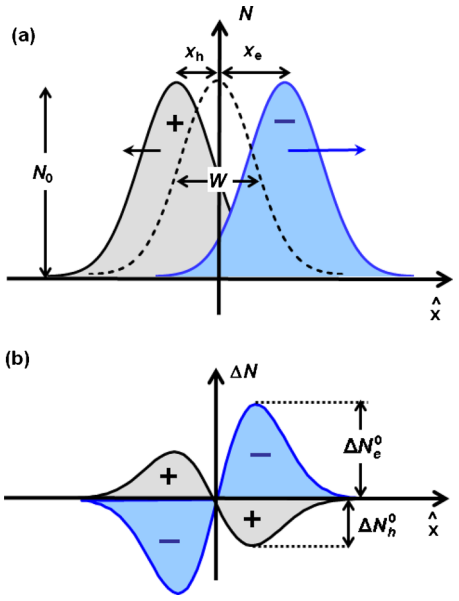

FIG. 2. (Color online) Schematic showing the injection of charge current by colinearly polarized (along $\hat{x}$) fundamental and second harmonic pump pulses with frequencies ω and 2ω, respectively. (a) The electrons and holes are initially injected by two and one photon absorption with an identical Gaussian spatial density profile (dashed curve of height N_0 and width W). For $\Delta\phi=3\pi/2$, the electrons (holes) move to the right (left) with average velocity $\langle v_e\rangle$ ($\langle v_h\rangle$). As a result, the electrons (holes) travel a distance x_e (x_h) in time t. (b) The differential change in the electron density ΔN_e (hole density ΔN_h) caused by the carrier motion depicted in (a).

$\langle v_{e(h)}(t=0)\rangle \sin \Delta\phi]$, and for the situation depicted in Fig. 2, x_e (x_h) is positive (negative).

Consequently, the problem of measuring the electron and hole motion following ballistic injection reduces to measuring $W(t)$, $N_0(t)$, and $\Delta N^0_{e(h)}(\Delta\phi;t)$. This motion is sketched in Fig. 2, assuming that the profiles shift rigidly. As suggested, the electrons and holes are injected in opposite directions with equal crystal momentum, and their contributions to the current add. Subsequently, the electron and hole spatial distributions separate until the injected momentum relaxes by electron-hole and carrier-phonon scattering.[21,22] As the electrons and holes separate, a space charge field, E_{sc}, develops, which opposes the separation of the electrons and holes. Eventually, the restoring force associated with E_{sc} causes the electrons and holes to return to a common position. In the next section, we describe *phase-independent* differential transmission techniques for measuring $W(t)$, $N_0(t)$, and in the following section, *phase-dependent* differential transmission techniques for measuring $\Delta N^0_{e(h)}(\Delta\phi;t)$.

III. CARRIER DENSITY SPATIAL PROFILES

The width $W(t)$ and height $N_0(t)$ are extracted from the electron and hole spatial profiles by measuring the conventional differential transmission of a probe pulse at 1500 nm. The probe is taken as the output signal of the OPO, is delayed with respect to the pump pulses, and is focused onto the back surface of the sample by a lens that is identical to the one used to focus the ω and 2ω pump pulses. Subsequently, the transmitted probe pulse is collimated, and directed to a photodiode. For the measurements described in this section, no current is injected ($\Delta\phi=0$). Instead, the pump beams are modulated using a mechanical chopper, and the probe transmission is detected using a lock-in amplifier tuned to the chopper frequency. In this way, the difference between the probe transmission with the pump present and the transmission without the pump present is measured as the probe is scanned across the sample surface. Taking into account the finite spatial probe profile, the measured differential transmission is of the form:

$$\Delta T(N;x,y;t)/T_0 = \int C(x-x',y-y')[T(0;x',y';t) - T_0]/T_0 dx'dy', \tag{3}$$

where $T(\Delta\phi=0;x,y;t)$ is the *local* transmission established at position x,y and time t by the ω and 2ω pump pulses in the absence of an current injection ($\Delta\phi=0$), and T_0 is the linear transmission of the sample in the absence of the pump pulses. The finite diameter Λ of the probe pulse is taken into account by the convolution of $(T-T_0)$ with

$$C(x,y) \equiv \frac{4\ln 2}{\pi\Lambda^2}\exp\left[-4\ln 2\left(\frac{x^2+y^2}{\Lambda^2}\right)\right], \tag{4}$$

which is normalized such that $\int C(x,y)dxdy=1$. Also, notice that for ideal focusing conditions, the probe diameter and the initial diameter of the carrier density profile are the same: $\Lambda=W(t=0)$. Finally, the notation $\Delta T(N)$ is meant to emphasize that the differential transmission $(T-T_0)$ described in this section is a function of the carrier density produced by the pumps and not dependent on the phases of the two pump pulses.

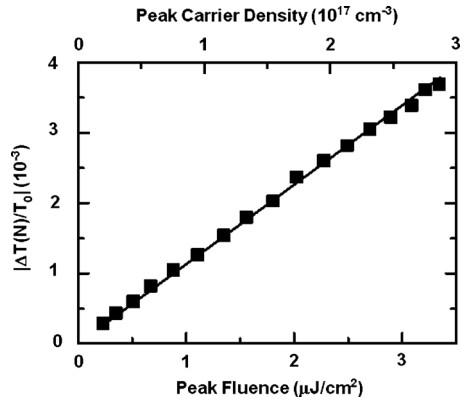

FIG. 3. Magnitude of the phase-independent differential transmission $\Delta T(N;x=0,\ y=0;t)/T_0$ for a fixed time delay of $\tau=0.52$ ps as a function of the 2ω pump pulse fluence. The upper axis gives the estimated carrier density.

The peak probe differential transmission, $\Delta T(N;0,0;t)/T_0$, is approximately a linear function of carrier density and is $\ll 1$ over the fluence range used here, although the slope varies as a function of time. An example is shown in Fig. 3 for a time delay of $t=0.52$ ps, where $\Delta T(N;0,0;t)/T_0$ is shown as a function of the 2ω fluence, with the ω beam blocked to ensure a linear dependence between pump fluence and carrier density. The upper axis is an estimate of the carrier density based on the linear absorption coefficient for 2ω given above (i.e., $\alpha^{2\omega}\sim 3\times 10^4$ cm^{-1}).[16] These characteristics allow the differential transmission to be written as:

$$\begin{aligned}[T(0;x,y;t)-T_0]/T_0 &= -\int \Delta\alpha dz \\ &= -\sigma_e(t)\int N_e(0;x,y;t)dz \\ &\quad -\sigma_h(t)\int N_h(0;x,y;t)dz, \\ &\cong -[\sigma_e(t)+\sigma_h(t)]\int N(0;x,y;t)dz,\end{aligned} \tag{5}$$

where the proportionality factors σ_e and σ_h are effective cross sections for the contributions of the electrons and holes, respectively, which are created by the pump, to the change in the absorption coefficient of the probe pulse. These cross sections are allowed to depend upon time to reflect the electron and hole relaxation within the valence and conduction band. The second approximate equality follows from setting $N(0;x,y;t)\equiv N_e(0;x,y;t)\cong N_h(0;x,y;t)$, which is allowed because $N_e(0;x,y;0)=N_h(0;x,y;0)$ and because diffusion and recombination are negligible on the <2 ps time scales of interest here (as we will discuss below). Within these approximations, Eq. (3) becomes

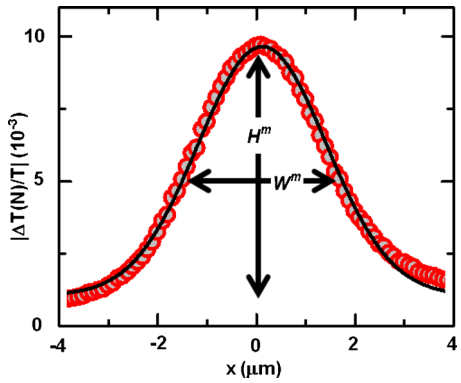

FIG. 4. (Color online) The magnitude of the phase-independent differential transmission $\Delta T(N;x,y=0;t)/T_0$ measured as a function of position along the x-axis ($y=0$) for a fixed time delay ($\tau=0.4$ ps) and for fixed ω (250 μJ/cm^2) and 2ω (5.5 μJ/cm^2) pump fluences. The measured height H^m and width W^m of the profile are extracted by fitting the data to a Gaussian (solid line).

$$\Delta T(N;x,y;t)/T_0 = -\sigma(t)\int C(x-x',y-y') \times N(0;x',y';t)dx'dy'dz, \quad (6)$$

where $\sigma=\sigma_e+\sigma_h$.

The spatial profile of the differential transmission $\Delta T(N;x,y=0;\ t=0.4\ \text{ps})/T_0$ measured by scanning the probe along the x-axis across the pump region at a fixed time delay is shown in Fig. 4. For these measurements, the 2ω pump (5.5 μJ/cm^2) is estimated to inject a peak density of $\sim 5\times 10^{17}$ cm^{-3} by one photon absorption, and the ω pump (250 μJ/cm^2) a density of $\sim 4\times 10^{16}$ cm^{-3} by two photon absorption and $\sim 3\times 10^{16}$ cm^{-3} by indirect absorption. The measured height $H^m \equiv \Delta T(N;0,0;t)/T_0$ and width W^m [defined as the FWHM of $\Delta T(N;x,0;t)/T_0$] of the profile are indicated.

To confirm that diffusion and recombination make negligible contributions to the carrier dynamics on the time scale of our experiments, we measure $H^m(t)$ and $W^m(t)$ as a function of time delay. The time required for diffusion to double $W^m(t)$ is $\sim$550 ps, and the time required for bulk and surface recombination and diffusion to reduce $H^m(t)$ to e^{-1} of its peak value is $\sim$200 ps.

Comparison with earlier work[1,5–8] indicates that the differential transmission shown in Fig. 4 is >10 times smaller than for similar experimental conditions in direct gap materials, such as GaAs. In GaAs, the probe is absorbed principally by direct one photon valence-to-conduction band transitions, and the differential signal is associated with a saturation of the direct absorption coefficient caused by phase space filling. Because of the smaller conduction band effective mass, the electrons in the conduction band of GaAs are more effective in blocking the direct transitions than the holes in the valence band. Consequently, in GaAs, the electrons make the dominant contribution to $\Delta T(N;x,0;t)/T_0$ (i.e., $\sigma_e \gg \sigma_h$), and it is the electronic motion that we follow.

Similar to the GaAs case, the probe energy $\hbar\omega$ used in our Ge studies is larger than the direct gap. Therefore, the dominant absorption process for the probe in Ge is also direct, and the measured change in the probe transmission is associated with the saturation of the direct transitions by electrons in the Γ-valley and holes in the valence band. Also, like GaAs, the effective mass of the conduction band for Ge is smaller than that for the valence band. Consequently, density of states arguments again suggest that the electrons are more effective than the holes in blocking the states needed for direct absorption (i.e., $\sigma_e \gg \sigma_h$)—so long as the electrons remain in the Γ-valley where they are initially deposited by the pump. However, in contrast to GaAs, which is a direct gap material where scattering to the side valleys is unlikely, Ge is indirect, and the electrons are known to scatter to the side valleys within 100–200 fs.[14,23] Once in the side valleys, the electrons no longer contribute significantly to the saturation of the direct absorption as seen by the probe pulse. Hence, in Ge, the differential transmission of the probe pulse is dominated by, and mainly follows, the holes for $t > 200$ fs.

IV. MEASUREMENT OF CARRIER TRANSPORT

The carrier transport is monitored by measuring the peak of derivativelike phase-dependent change in carrier density $\Delta N_{e(h)}(\Delta\phi;x,y;t)$, as discussed in Sec. II. The peak of $\Delta N_{e(h)}(\Delta\phi;x,y;t)$, in turn, is extracted by measuring the phase-dependent differential transmission. For these measurements, the chopper used in the differential transmission measurements described in the previous section is removed. Instead, a piezoelectric transducer in one arm of the interferometer dithers $\Delta\phi$ about its set value, and the phase-dependent change in transmission is measured by slaving the lock-in amplifier to the piezoelectric transducer. Again, taking into account the finite spatial probe profile, the measured phase-dependent differential transmission can be written:

$$\frac{\delta T(\Delta\phi;x,y;t)}{T} = \frac{\int C(x-x',y-y')[T(\Delta\phi;x',y';t)-T(0;x',y';t)]dx'dy'}{\int C(0-x',0-y')T(0;x',y';t)dx'dy'}. \quad (7)$$

Using a $\Delta\phi$-dependent version of Eq. (5), this expression can be rewritten in terms of the phase-dependent changes in electron and hole densities:

$$\delta T(\Delta\phi;x,y;t)/T = -\int C(x-x',y-y') \times \begin{bmatrix} \sigma_e(t)\Delta N_e(\Delta\phi;x',y';t) \\ +\sigma_h(t_h)\Delta N_h(\Delta\phi;x',y';t) \end{bmatrix} dx'dy'dz, \quad (8)$$

where we have neglected the small change in transmission ($<10^{-2}$) caused by the electrons and holes in evaluating the denominator in Eq. (7).

We emphasize that $\delta T(\Delta\phi;x,y;t)/T$ is the normalized difference between the transmissions with current injection ($\Delta\phi\neq 0$) and without the current injection ($\Delta\phi=0$), as opposed to Eq. (3), which is the difference between transmissions with and without the pumps present ($\Delta\phi=0$ always). In contrast to $\Delta T(N;x,y;t)/T$, the pumps are always present when $\delta T(\Delta\phi;x,y;t)/T$ is measured. Furthermore, only

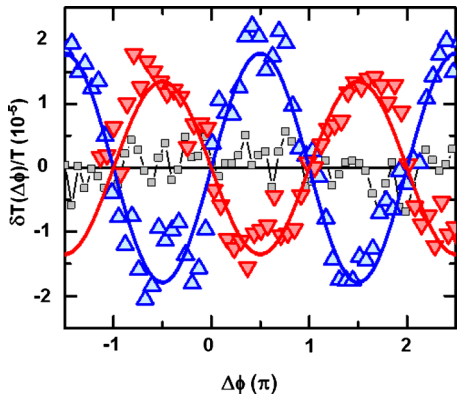

FIG. 5. (Color online) The phase-dependent differential transmission $\delta T(\Delta\phi;x,y=0;t)/T$ at a fixed time delay (τ=0.4 ps) at positions x= +1.1 μm (up-triangles), 0 (squares), and −1.1 μm (down triangles) as function of $\Delta\phi$.

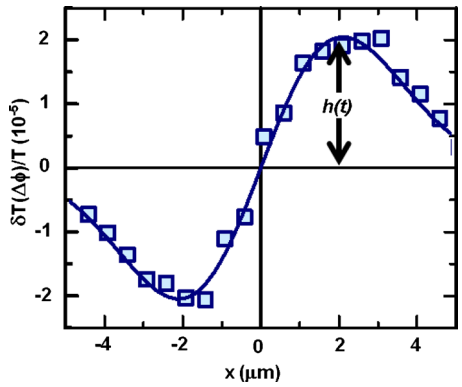

FIG. 6. (Color online) Spatial profile of the phase-dependent differential transmission $\delta T(\Delta\phi;x,y=0;t)/T$ measured for a fixed phase ($\Delta\phi=\pi/2$) and fixed probe delay of 0.4 ps. The measured peak height $h^m(t)$ is extracted by fitting the data to the derivative of a Gaussian (solid line).

$\Delta\phi$-dependent signals are passed by the lock-in amplifier and appear in Eqs. (7) and (8). Not only are changes in carrier density caused by processes such as diffusion and recombination negligible on time scales of a few picosecond but they are independent of phase and will not be passed by the lock-in.

The dependence of $\delta T(\Delta\phi;x,y=0;\ t=0.4\ \text{ps})/T$ on the relative phase of the ω and 2ω pump pulses is shown in Fig. 5 for a fixed time delay of τ=0.4 ps and for three distinct probe positions along the x-axis: x=+1.5 μm (up-triangles), 0 μm (squares), and −1.5 μm (down triangles)]. For these measurements, the 2ω and ω pump pulse fluences are the same as for Fig. 4. Notice that $\delta T/T$ varies sinusoidally with $\Delta\phi$. When $\sin\Delta\phi>0$, $\delta T(\Delta\phi;x,y=0;\ t=4\ \text{ps})/T$ increases on one side of the sample (at x=+1.1 μm) and decreases on the other (at x=−1.1 μm), and when $\sin\Delta\phi<0$, the positions at which the transmission increases and decreases are reversed. Maxima and minima are observed when $\Delta\phi$ is an odd multiple of $\pi/2$. No measurable increase or decrease in transmission is observed at x=0 for any phase.

Measurements similar to those depicted in Fig. 5 are performed for a more extensive set of positions along the x-axis. At each position, $\delta T(\Delta\phi;x,y=0;\ t=0.4\ \text{ps})/T$ is fit with a sine function. The amplitude $\delta T(\pi/2;x,y=0;\ t=0.4\ \text{ps})/T$ is plotted versus position in Fig. 6. For this phase and at this time, the figure indicates an accumulation of carriers on the right and a depletion on the left. The behavior shown in Figs. 5 and 6 is consistent with the discussions of Sec. II and confirms that interference between one photon absorption of 2ω and two photon absorption of ω pulses injects a phase-dependent charge current in Ge.

In order to estimate the average distance moved per carrier in Ge, it is convenient to first use Eqs. (1), (5), and (6) to rewrite $\delta T(\Delta\phi)/T$ in terms of $\Delta T(N)/T$:

$$\frac{\delta T(\Delta\phi;x,y;t)}{T}=-\left[\frac{\sigma_h(t)x_h+\sigma(t)x_e}{\sigma(t)+\sigma(t)}\right]\frac{\partial}{\partial x}\left[\frac{\Delta T(N;x,y;t)}{T_0}\right]. \tag{9}$$

If $\Delta T(N;x,0;t)/T_0$ can be fit by a Gaussian of height $H^m(t)$ and FWHM $W^m(t)$ (e.g., see Fig. 4), then it is straight forward to define a parameter $\langle x\rangle$ such that

$$\langle x\rangle\equiv\left[\frac{\sigma_h(t)x_h+\sigma_e(t)x_e}{\sigma_h(t)+\sigma_e(t)}\right]=\frac{1}{2}\sqrt{\frac{e}{2\ln 2}}\left[\frac{h^m(t)}{H^m(t)}\right]W^m(t), \tag{10}$$

where $h^m(t)$ is defined as the peak phase-dependent differential transmission, which is obtained by evaluating $\delta T(\Delta\phi)/T$ at the inflection point of the Gaussian:

$$h^m(t)\equiv\delta T[\Delta\phi;x=W^m(t)/[2\sqrt{2\ln 2}],y=0;t]/T. \tag{11}$$

The parameter $\langle x\rangle$ has units of distance and, effectively, is the average distance moved by the electrons plus the holes weighted by the sensitivity of the probe to each species. Said another way, the expression for $\langle x\rangle$ resembles that for a "*center of mass*" coordinate except that the electron and hole positions are weighted by σ_e and σ_h, rather than by an effective mass. A number of characteristics of $\langle x\rangle$ are of interest. First, if the probe were equally sensitive to electrons and holes ($\sigma_e=\sigma_h$) and if they were to move the same distance in opposite directions (i.e., $x_e=-x_h$), $\langle x\rangle=0$. Consequently, oppositely-directed hole motion tends to subtract from the electron movement in determining $\langle x\rangle$. If the probe is sensitive primarily either to the electrons ($\sigma_e\gg\sigma_h$) or to the holes ($\sigma_e\ll\sigma_h$), then the cross sectional dependence cancels, Eq. (10) reduces to Eq. (2), and $\langle x\rangle$ corresponds to either x_e or x_h. In our previous experiments in GaAs,[1,5–8] the probe was sensitive to the electrons ($\sigma_e>\sigma_h$). Here, we speculate that the probe primarily detects electrons while they remain in the central Γ conduction band valley (times ≤200 fs), and detects the holes ($\sigma_e<\sigma_h$) once the electrons scatter to the side valleys.

Extracting values for $H^m(t)$, $h^m(t)$, and $W^m(t)$ from Figs. 5 and 6, we calculate $\langle x\rangle\sim 7$ nm at t=0.4 ps under the excitation conditions described here. The result of repeating these measurements as a function of time delay is summarized in Fig. 7. The temporal behavior of $\langle x\rangle$ is consistent with the dynamics depicted in Fig. 2. Following injection with oppositely directed average ballistic velocities $\langle v_{e(h)}(t=0)\rangle$, the electrons and holes initially move apart. As they separate, momentum relaxation destroys the ballistic velocities, and a space charge field forms that opposes the separa-

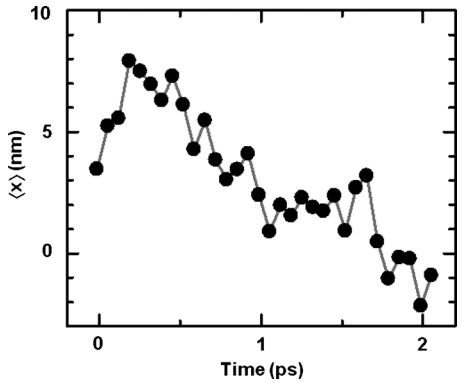

FIG. 7. The effective average shift $\langle x \rangle$ of the electrons and holes (solid circles) as extracted from the measurements of H^m, W^m, and h^m.

tion. Eventually (~2 ps), the space charge field causes the electrons and holes to return to approximately their original positions.

V. SUMMARY AND DISCUSSION

We have demonstrated the all-optical injection of ballistic charge currents in germanium at room temperature by two color QUIC techniques. The charge transport following injection is monitored using tightly-focused phase-sensitive differential transmission techniques with femtosecond temporal and nm spatial resolution. The carrier dynamics are determined by competition between the ballistic injection current and the space charge fields that develop as the result of the separation of the electrons and holes.

From a quantum interference point of view, Ge functions as a direct gap material, but its indirect nature complicates the carrier dynamics and the monitoring of the carrier transport. The electrons and holes are initially deposited in the central valley of the conduction band and the valence band, respectively, with large excess ballistic velocities by quantum interference between *direct* one and two photon absorption of the pump pulses. Until momentum relaxes the ballistic motion, the electrons remain in the Γ valley, and because of its small effective mass, the electrons dominate the measured differential transmission. On the time scale of the momentum relaxation, the electrons thermalize and transfer to the side valleys, where they move with a reduced effective mass and have a negligible effect on the direct absorption of the probe. Because of this transfer, the probe primarily monitors the hole transport, as dictated by the space charge field—where the space charge field dynamics are determined by the reduced side valley electronic effective mass.

All of the measurements reported here for Ge are much noisier than the corresponding measurements in GaAs. The signals are noisier not because the quantum interference process is weaker in Ge; rather, they are noisier because the differential transmission signals are roughly an order of magnitude smaller than in GaAs, pushing our detection limits. There are at least two reasons why the probe differential signal is weaker in Ge. First, the signals are smaller because Ge is an indirect band gap material. As discussed in the previous paragraph, because of the absence of carriers in the central valley, the holes play a bigger role in determining the differential transmission in Ge, and because of their larger effective mass (compared to the electrons in the central valley of either GaAs or Ge), the holes move a shorter distance and are less effective in blocking the direct transitions for the probe pulse. Consequently, the differential transmission is reduced by at least an order of magnitude in Ge compare to GaAs.

The second reason that the differential signal is smaller in Ge than in GaAs is because the injection process is not balanced in the experiment reported here. The quantum interference between one and two photon absorption is most efficient when each process produces the same number of carriers. Because of experimental constraints related to the tuning and power of the OPO, we were unable to produce the same generation rate for two photon absorption of the ω pulse as for one photon absorption of the 2ω pulse. Consequently, a smaller fraction of the carriers participate in the ballistic charge current for a given total density, reducing the average velocity of electrons and holes.

ACKNOWLEDGMENTS

We acknowledge insightful discussions with Henry van Driel, Julien Rioux, and John Sipe. This work was supported in part by NSF, ONR, and DARPA.

[1] H. Zhao, E. J. Loren, A. L. Smirl, and H. M. van Driel, J. Appl. Phys. **103**, 053510 (2008).
[2] R. Atanasov, A. Hache, J. L. P. Hughes, H. M. van Driel, and J. E. Sipe, Phys. Rev. Lett. **76**, 1703 (1996).
[3] A. Haché, Y. Kostoulas, R. Atanasov, J. L. P. Hughes, J. E. Sipe, and H. M. van Driel, Phys. Rev. Lett. **78**, 306 (1997).
[4] R. D. R. Bhat and J. E. Sipe, Phys. Rev. Lett. **85**, 5432 (2000).
[5] M. J. Stevens, A. L. Smirl, R. D. R. Bhat, J. E. Sipe, and H. M. van Driel, J. Appl. Phys. **91**, 4382 (2002).
[6] M. J. Stevens, A. Najmaie, R. D. R. Bhat, J. E. Sipe, H. M. van Driel, and A. L. Smirl, J. Appl. Phys. **94**, 4999 (2003).
[7] H. Zhao, E. J. Loren, H. M. van Driel, and A. L. Smirl, Phys. Rev. Lett. **96**, 246601 (2006).
[8] Y. Kerachian, P. A. Marsden, H. M. van Driel, and A. L. Smirl, Phys. Rev. B **75**, 125205 (2007).
[9] Y.-H. Kuo, Y. K. Lee, Y. Ge, S. Ren, J. E. Roth, T. I. Kamins, D. A. B. Miller, and J. S. Harris, Nature (London) **437**, 1334 (2005).
[10] J. Liu, X. Sun, L. C. Kimerling, and J. Michel, Opt. Lett. **34**, 1738 (2009).
[11] C. Lange, N. S. Köster, S. Chatterjee, H. Sigg, D. Chrastina, G. Isella, H. von Känel, M. Schäfer, M. Kira, and S. W. Koch, Phys. Rev. B **79**, 201306 (2009).
[12] M. Spasenović, M. Betz, L. Costa, and H. M. van Driel, Phys. Rev. B **77**, 085201 (2008).
[13] T. Rappen, U. Peter, M. Wegner, and W. Shäfer, Phys. Rev. B **48**, 4879 (1993).
[14] G. Mak and H. M. van Driel, Phys. Rev. B **49**, 16817 (1994).
[15] X. Q. Zhou, H. M. van Driel, and G. Mak, Phys. Rev. B **50**, 5226 (1994).
[16] W. C. Dash and R. Newman, Phys. Rev. **99**, 1151 (1955).
[17] E. W. van Stryland, Y. Y. Wu, D. J. Hagan, M. J. Soileau, and K. Mansour, J. Opt. Soc. Am. B **5**, 1980 (1988).
[18] J. I. Pankove and P. Aigrain, Phys. Rev. **126**, 956 (1962).
[19] A. Najmaie, R. D. R. Bhat, and J. E. Sipe, Phys. Rev. B **68**, 165348 (2003).
[20] R. D. R. Bhat and J. E. Sipe, arXiv:cond-mat/0601277 (unpublished).
[21] H. T. Duc, T. Meier, and S. W. Koch, Phys. Rev. Lett. **95**, 086606 (2005).
[22] W. A. Hügel, M. F. Heinrich, M. Wegener, Q. T. Vu, L. Bányai, and H. Haug, Phys. Rev. Lett. **83**, 3313 (1999).
[23] C. Lange, N. S. Köster, S. Chatterjee, H. Sigg, D. Chrastina, G. Isella, H. von Känel, B. Kunert, and W. Stolz, Phys. Rev. B **81**, 045320 (2010).